SUPPORTING INFORMATION

Optimal-tuning of Range-Separated Density Functional to describe optical and photophysical properties of Rhodamine B dimers

Giacomo Fanciullo[1], Carlo Adamo[2], Ivan Rivalta*[1,3], Ilaria Ciofini*[2]

[1] Dipartimento di Chimica Industriale "Toso Montanari", Alma Mater Studiorum, Università di Bologna, Viale del Risorgimento 4, 40136 Bologna, Italy.

[2] Chimie ParisTech, PSL University, CNRS, Institute of Chemistry for Life and Health Sciences, Chemical Theory and Modelling Group, F-75005 Paris, France.

[3] CNRS, Laboratoire de Chimie UMR 5182, 46 Allée d'Italie, 69364 Lyon, France.

S.1. INPUTS FOR RANGE-SEPARATION

In the following are reported few examples of IOps related to some of the functionals employed in this work

Example 1: γ = 0.18, 0% SR HF eX (α = 0.00) and 100% LR HF eX (β = 1.00).

Input:

```
IOp(3/107=0180000000) IOp(3/108=0180000000) IOp(3/119=1000000000)
IOp(3/120=1000000000) IOp(3/130=-1) IOp(3/131=-1)
```

Example 2: γ = 0.13, 28% SR HF eX (α = 0.28) and 44% LR HF eX (β = 0.16) (Diox screening).

Input:

```
IOp(3/107=0130000000) IOp(3/108=0130000000) IOp(3/119=0160000000)
IOp(3/120=0160000000) IOp(3/130=02800) IOp(3/131=02800)
```

Example 3: γ = 0.13, 29% SR HF eX (α = 0.29) and 3% LR HF eX (β = -0.26) (AcN screening).

Input:

```
IOp(3/107=0130000000) IOp(3/108=0130000000) IOp(3/119=0260000000)
IOp(3/120=0260000000) IOp(3/130=1202900) IOp(3/131=1202900)
```

S.2. ADDITIONAL RESULTS

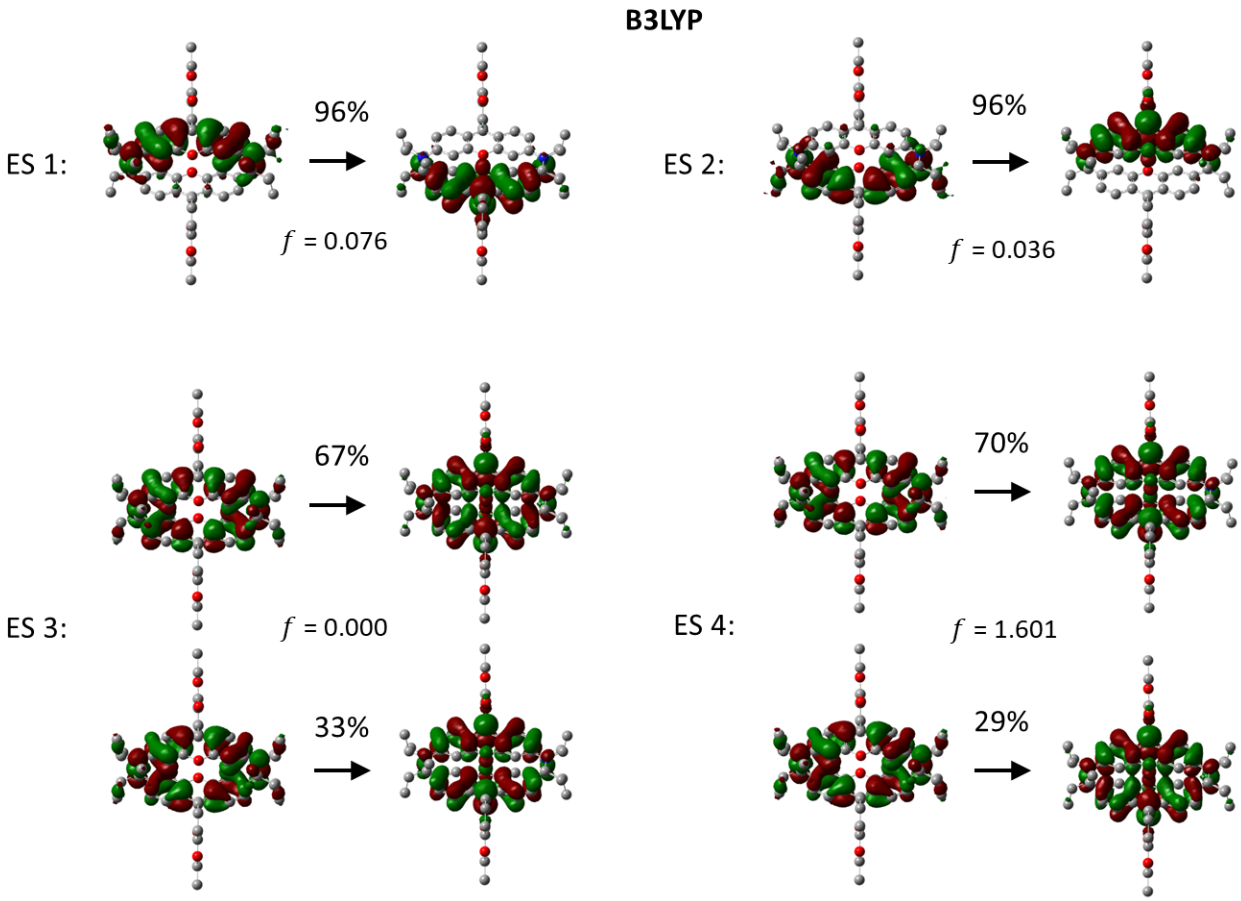

Figure S1. NTOs describing the lowest ESs predicted by B3LYP for the H dimer in Diox (they are representative also for AcN).

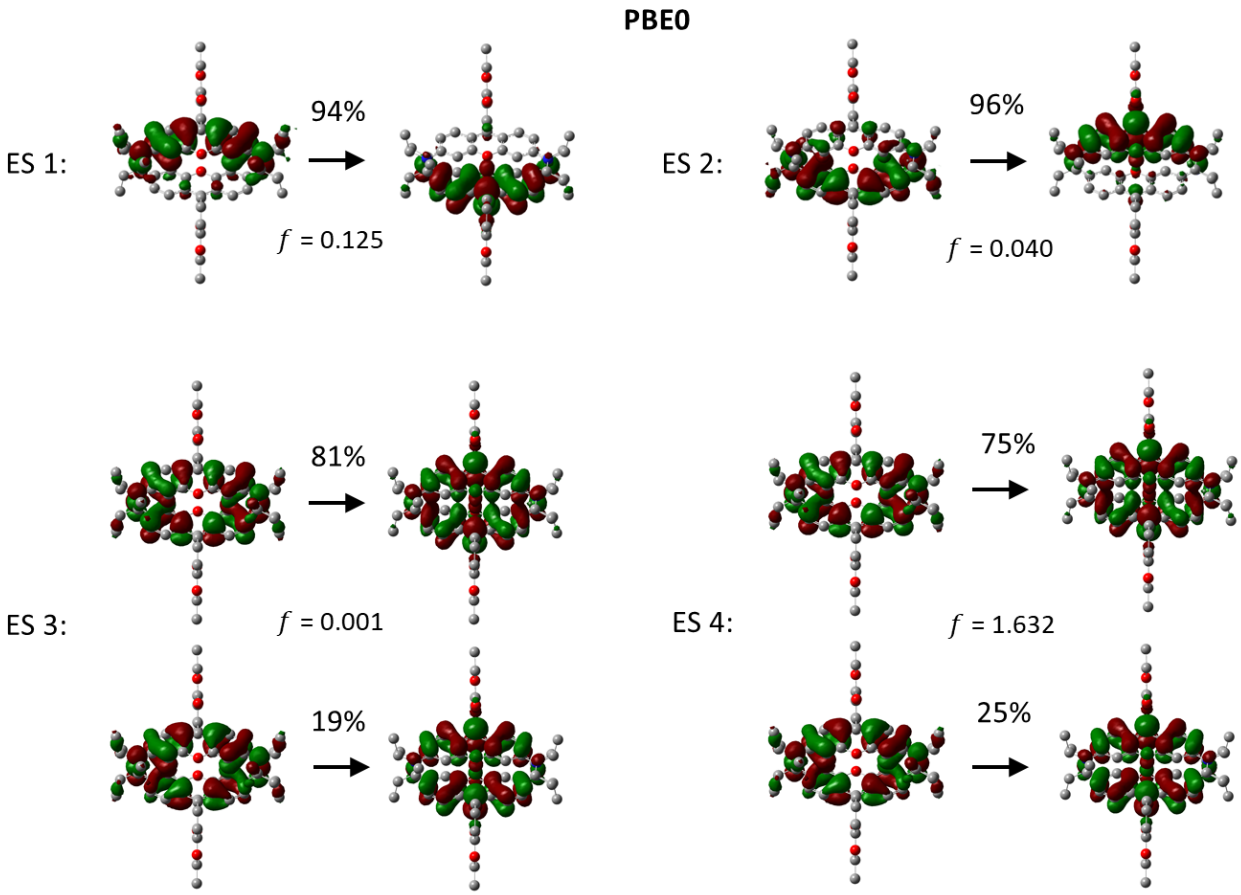

Figure S2. NTOs describing the lowest ESs predicted by PBE0 for the H dimer in Diox (they are representative also for AcN).

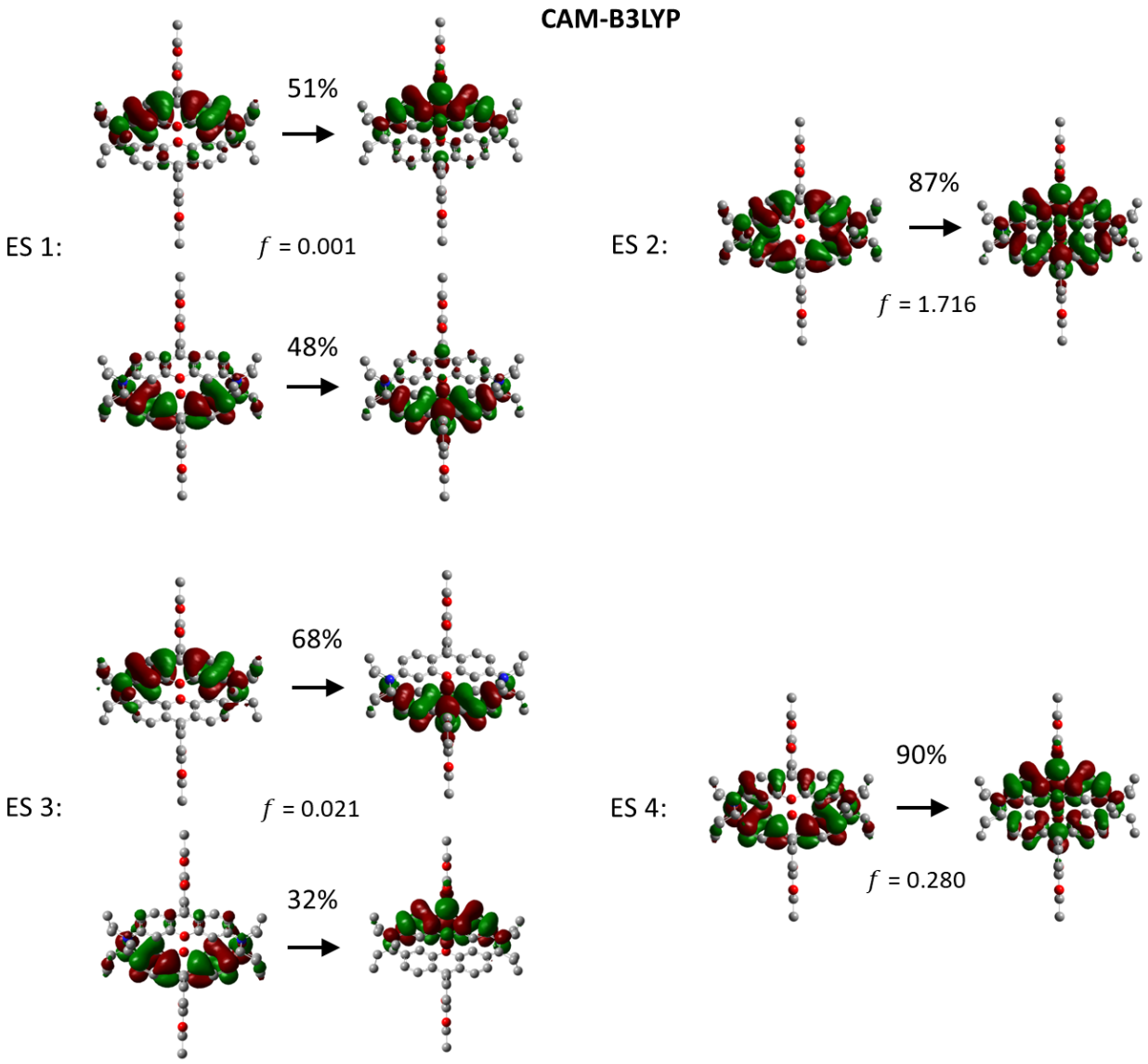

Figure S3. NTOs describing the lowest ESs predicted by CAM-B3LYP for the H dimer in Diox (they are representative also for AcN).

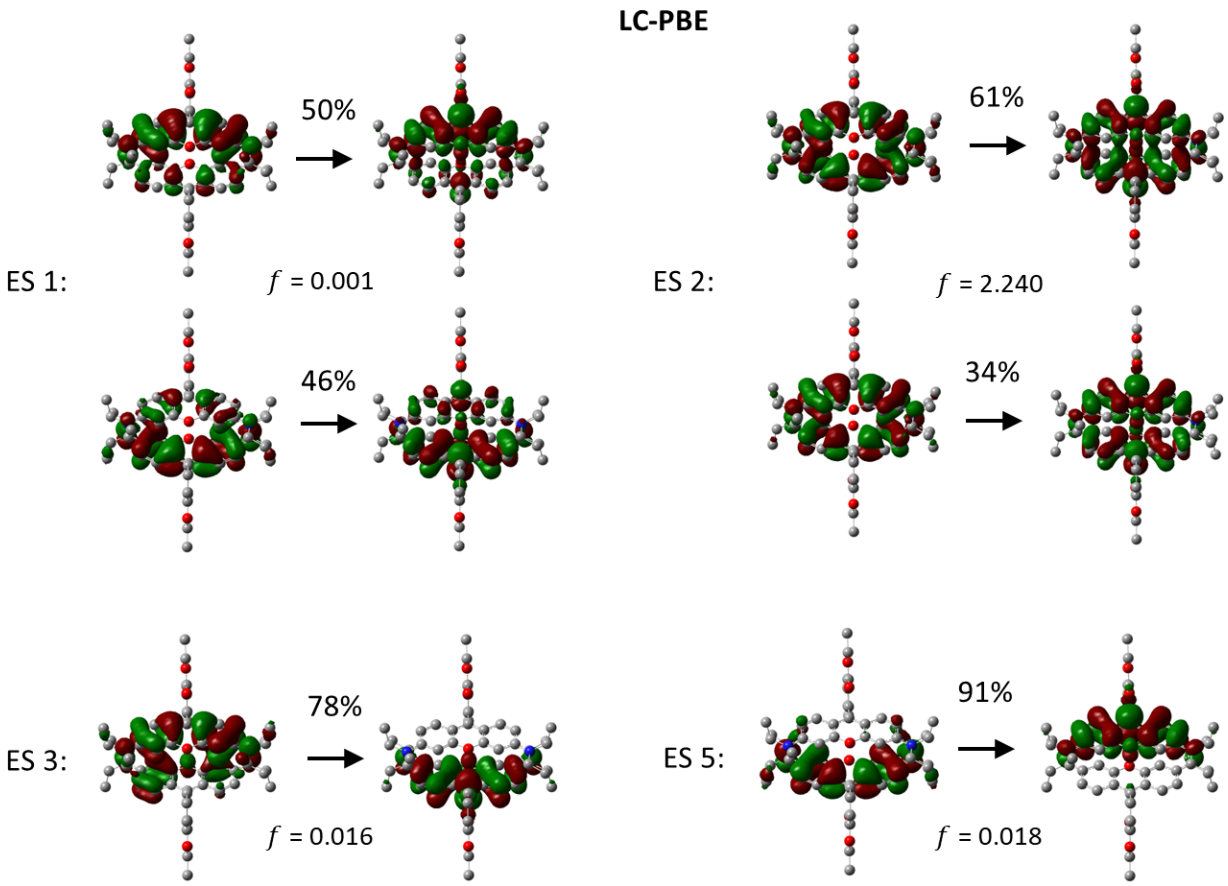

Figure S4. NTOs describing the lowest ESs predicted by LC-PBE for the H dimer in Diox (they are representative also for AcN).

	f in AcN	
	CT 1	CT 2
B3LYP	0.062 (4.0%)	0.035 (2.2%)
PBE0	0.100 (6.2%)	0.041 (2.5%)
CAM-B3LYP	0.027 (1.7%)	0.312 (19.2%)
LC-PBE	0.006 (0.3%)	0.022 (1.0%)

Table S1. Oscillator strengths (f, in a.u.) of the H dimer's CT states predicted by standard functionals in AcN. The percentage in parenthesis indicates the relative magnitude of f calculated with respect to the bright DE state at the same level of theory.

	α = 0.0 β = 1.0		α = 0.1 β = 0.9		α = 0.2 β = 0.8		α = 0.3 β = 0.7		α = 0.4 β = 0.6	
	γ*	J_{min}(eV)	γ*	J_{min}(eV)	γ*	J_{min}(eV)	γ*	J_{min}(eV)	γ*	J_{min}(eV)
V-CAM-B3LYP*	0.18	0.051	0.16	0.046	0.13	0.020	0.11	0.028	0.08	0.039
V-LC-PBE*	0.18	0.051	0.16	0.047	0.13	0.020	0.11	0.036	0.08	0.050

Table S2. Optimal γ values (bohr^{-1}) and minimum values of $\sqrt{J_V^2}$ (indicated as J_{min}) obtained for the V-RSH* functionals starting from different (α, β) couples and using the 6-31G* basis set. The γ-scan has been performed through variations limited to 0.01 bohr^{-1}.

	α = 0.0 β = 1.0		α = 0.1 β = 0.9		α = 0.2 β = 0.8		α = 0.3 β = 0.7		α = 0.4 β = 0.6	
	γ*	J_{min}(eV)	γ*	J_{min}(eV)	γ*	J_{min}(eV)	γ*	J_{min}(eV)	γ*	J_{min}(eV)
V-CAM-B3LYP*	0.17	0.050	0.15	0.037	0.13	0.037	0.10	0.010	0.07	0.037

Table S3. Optimal γ values and minimum values of the $\sqrt{J_V^2}$ function (indicated as J_{min}) obtained for the V-CAM-B3LYP* with the 6-311+G* basis set starting from different α, β couples. The γ-scan has been performed through variations limited to 0.01 bohr^{-1}.

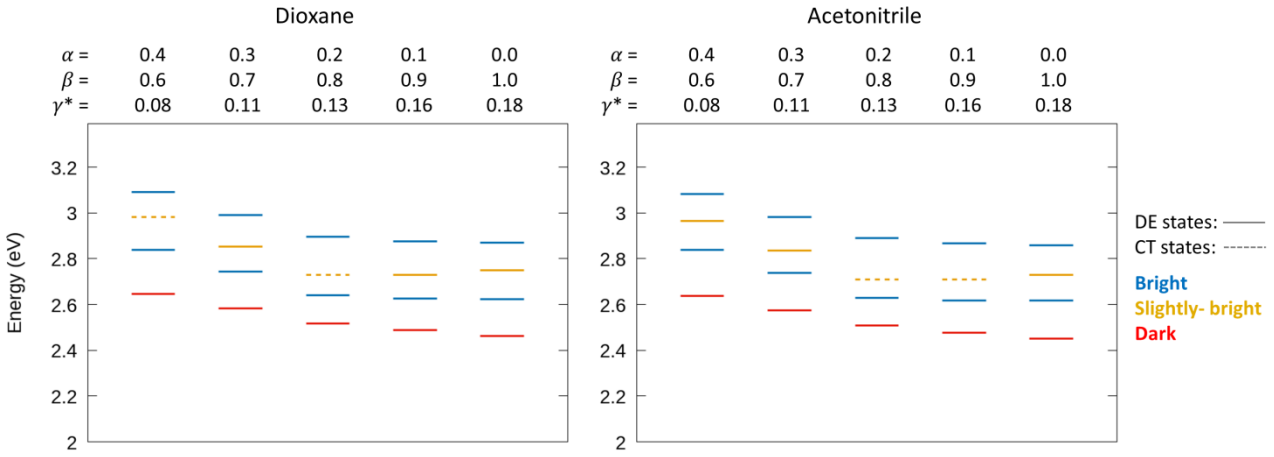

Figure S5. ES energy diagram predicted for the H dimer by the various V-LC-PBE* in both Diox (left) and AcN (right). For each state are also indicated the corresponding character (DE states with full lines, CT states with dashed lines) and brightness (bright states in blue, slightly bright states in orange, dark states in red, see Section 2 for details).

V-CAM-B3LYP*	f in Diox		f in AcN	
	ES 2	ES 4	ES 2	ES 4
α = 0.0, β = 1.0, γ* = 0.18	0.801	0.922	0.697	0.973
α = 0.1, β = 0.9, γ* = 0.16	0.831	0.948	0.723	1.002
α = 0.2, β = 0.8, γ* = 0.13	0.730	1.092	0.641	1.130
α = 0.3, β = 0.7, γ* = 0.11	1.005	0.902	0.884	0.968
α = 0.4, β = 0.6, γ* = 0.08	1.304	0.686	1.181	0.752

Table S4. Oscillator strengths (f, in a.u.) of the 2nd and 4th ESs predicted for the H dimer by different V-CAM-B3LYP* functionals in different solvents.

V-LC-PBE*	f in Diox		f in AcN	
	ES 2	ES 4	ES 2	ES 4
α = 0.0, β = 1.0, γ* = 0.18	0.935	0.818	0.822	0.877
α = 0.1, β = 0.9, γ* = 0.16	0.781	1.010	0.673	1.063
α = 0.2, β = 0.8, γ* = 0.13	0.680	1.154	0.580	1.202
α = 0.3, β = 0.7, γ* = 0.11	0.941	0.981	0.819	1.048
α = 0.4, β = 0.6, γ* = 0.08	1.237	0.769	1.108	0.843

Table S5. Oscillator strengths (f, in a.u.) of the 2nd and 4th ESs predicted for the H dimer by different V-CAM-B3LYP* functionals in different solvents.

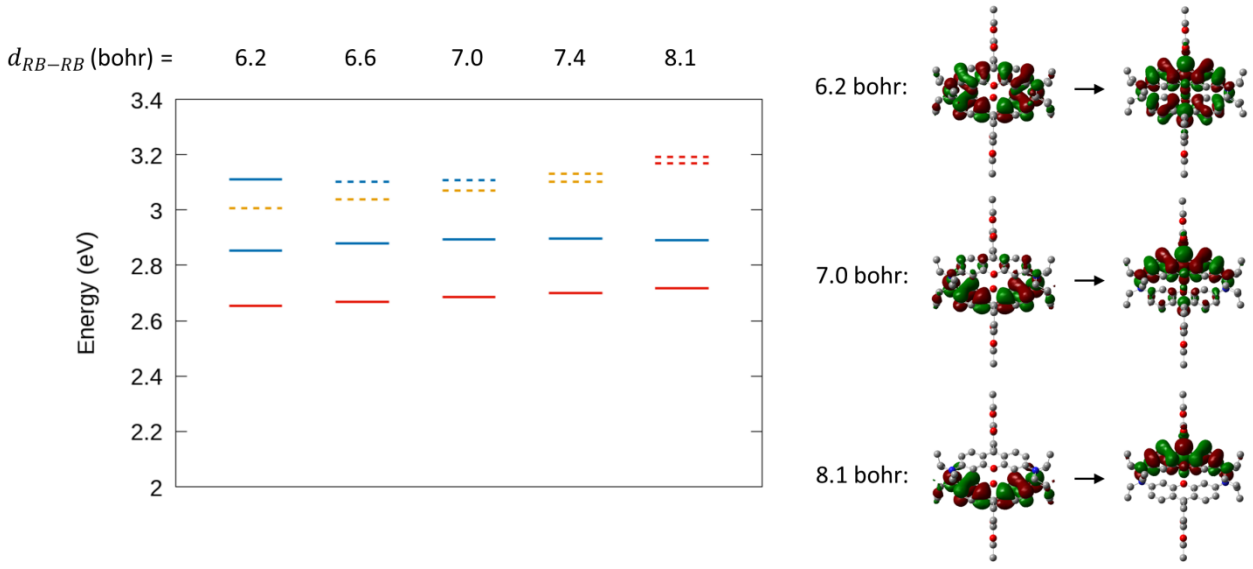

Figure S6. Energy diagram of the lowest ESs predicted for the H dimer by V-CAM-B3LYP* (α = 0.40, β = 0.60 and γ*= 0.08) evolving upon increasing d_{RB-RB} in Diox. The NTOs related to the 4th ES at selected distances are also reported.

	f	
d_{RB-RB} (Bohr)	$\alpha = 0.0$ $\beta = 1.0$ $\gamma^* = 0.18$	$\alpha = 0.40$ $\beta = 0.60$ $\gamma^* = 0.08$
6.2	0.801 (87.0%)	0.686 (52.6%)
6.6	0.735 (72.6%)	0.453 (29.1%)
7.0	0.410 (30.0%)	0.207 (11.3%)
7.4	0.136 (8.2%)	0.068 (3.4%)
8.1	0.009 (0.5%)	0.007 (0.3%)

Table S6. Oscillator strength (f, in a.u.) predicted by different versions of V-CAM-B3LYP* for the 4th ES of the H dimer in Diox upon increasing d_{RB-RB}. The percentage in parenthesis indicates the relative magnitude of f calculated with respect to the 2nd ES.

Diox	γ = 0.18		γ = 0.16		γ = 0.13		γ = 0.11		γ = 0.08	
	α^*	J_{min}(eV)	α^*	J_{min}(eV)	α^*	J_{min}(eV)	α^*	J_{min}(eV)	α^*	J_{min}(eV)
S-CAM-B3LYP*	0.23	0.008	0.25	0.009	0.28	0.019	0.30	0.019	0.32	0.018
S-LC-PBE*	0.23	0.013	0.25	0.014	0.28	0.016	0.30	0.021	0.32	0.025

Table S7. Optimal α values and minimum values of $\sqrt{J_S^2}$ (indicated as J_{min}) obtained for different S-RSH* functionals tuned within Diox starting from different γ values and using the 6-31G* basis set. The α-scan has been performed through variations limited to 0.01 bohr^{-1}.

AcN	γ = 0.18		γ = 0.16		γ = 0.13		γ = 0.11		γ = 0.08	
	α^*	J_{min}(eV)	α^*	J_{min}(eV)	α^*	J_{min}(eV)	α^*	J_{min}(eV)	α^*	J_{min}(eV)
S-CAM-B3LYP*	0.36	0.038	0.33	0.034	0.29	0.028	0.27	0.023	0.23	0.016
S-LC-PBE*	0.36	0.043	0.33	0.038	0.29	0.031	0.27	0.025	0.23	0.019

Table S8. Optimal α values and minimum values of $\sqrt{J_S^2}$ (indicated as J_{min}) obtained for different S-RSH* functionals tuned within AcN starting from different γ values and using the 6-31G* basis set. The α-scan has been performed through variations limited to 0.01 bohr^{-1}.

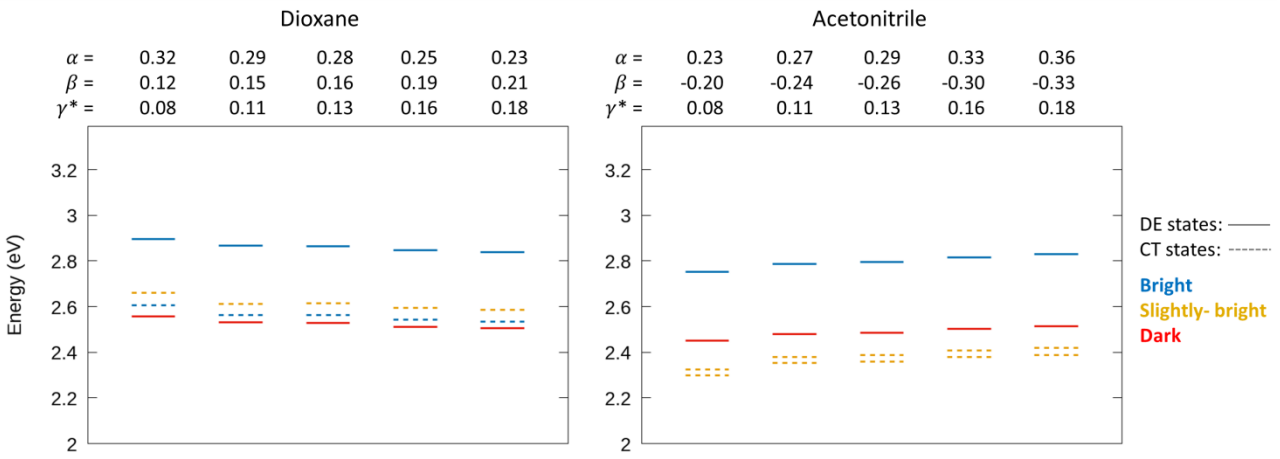

Figure S7. ES energy diagram predicted for the H dimer by the various S-LC-PBE* in both Diox (left) and AcN (right). For each state are also indicated the corresponding character (DE states with full lines, CT states with dashed lines) and brightness (bright states in blue, slightly bright states in orange, dark states in red, see Section 2 for details).

	f in Diox			
	S-CAM-B3LYP*		S-LC-PBE*	
	CT 1	CT 2	CT 1	CT 2
α* = 0.23, β* = 0.21, γ = 0.18	0.320 (21.6%)	0.031 (2.1%)	0.300 (19.8%)	0.023 (1.5%)
α* = 0.25, β* = 0.19, γ = 0.16	0.319 (21.4%)	0.033 (2.2%)	0.299 (19.7%)	0.025 (1.6%)
α* = 0.28, β* = 0.16, γ = 0.13	0.332 (22.2%)	0.036 (2.4%)	0.310 (20.2%)	0.029 (1.9%)
α* = 0.29, β* = 0.15, γ = 0.11	0.322 (21.3%)	0.037 (2.4%)	0.300 (19.4%)	0.029 (1.9%)
α* = 0.32, β* = 0.12, γ = 0.08	0.381 (25.7%)	0.040 (2.7%)	0.352 (16.6%)	0.034 (2.2%)
	f in AcN			
	S-CAM-B3LYP*		S-LC-PBE*	
	CT 1	CT 2	CT 1	CT 2
α* = 0.36, β* = -0.33, γ = 0.18	0.088 (5.3%)	0.034 (2.0%)	0.082 (4.9%)	0.032 (1.9%)
α* = 0.33, β* = -0.30, γ = 0.16	0.088 (5.3%)	0.034 (2.1%)	0.082 (4.9%)	0.032 (1.9%)
α* = 0.29, β* = -0.26, γ = 0.13	0.087 (5.3%)	0.034 (2.1%)	0.081 (4.9%)	0.032 (1.9%)
α* = 0.27, β* = -0.24, γ = 0.11	0.088 (5.4%)	0.034 (2.1%)	0.081 (5.0%)	0.032 (2.0%)
α* = 0.23, β* = -0.20, γ = 0.08	0.075 (4.7%)	0.032 (2.0%)	0.069 (4.3%)	0.031 (1.9%)

Table S9. Oscillator strengths (f, in a.u.) of the H dimer's CT states predicted S-RSH* functionals tuned in different solvents. The percentage in parenthesis indicates the relative magnitude of f calculated with respect to the bright DE state at the same level of theory.

ES	B3LYP (Diox)	CAMB3LYP (Diox)	PBE0 (Diox)	LC-PBE (Diox)	V-CAMB3LYP* (Diox)	S-CAMB3LYP* (Diox)	S-CAMB3LYP* (AcN)
1	3.351	0.035	3.216	0.031	0.022	0.083	3.306
2	3.331	0.130	3.112	0.030	0.635	2.162	3.298
3	0.066	1.832	0.229	2.551	0.277	2.157	0.029
4	0.053	1.904	0.061	3.244	0.338	0.104	0.040

Table S10: Computed D^{CT} values (in Å) corresponding to the first 4 excited states of RB dimer.

S.3. ORIGIN OF THE CT DELOCALIZATION

In this section it is presented the detailed analysis on how the interplay between α, β and γ RS parameters modulates the CT delocalization in the H dimer. As discussed in the main text, specific values of the RS parameters can provoke the formation of delocalization tails in the NTOs describing the CT excitations, which determine an increase of f for one of the two CT states. Therefore, the parameter that has been chosen for quantifying the CT delocalization is the f value related to this reference state.

The analysis consists in monitoring the reference state's f upon scanning each one of the RS parameters by keeping constant the other two. When a specific α, β, γ triad leads to a delocalization so high that the CT character is no longer recognisable, the reference state has been identified basing on its energetic evolution through the scan (in most of cases, the CT character can be recognized in the points of the scan that precede or follow the point at which the CT completely disappear). Since we found that neither the kind of DFT eX nor the solvent affects the ES picture, we limited our analysis to CAM-B3LYP and Diox.

The simultaneous effect of all the three RS parameters has been represented by means of sigmoidal functions aimed at qualitatively describing the variation the HF eX as a function of the inter-electronic distance.

We start the analysis by considering the α + β = 1 condition with α = 0. The f's evolution obtained upon scanning γ is reported in Figure S8 (Panel B) along with the modification of the ES manifold (Panel C) and the NTOs corresponding to the reference state (Panel D). The evident outcome is that the CT reference state becomes strongly bright when the switching distance is between 3 and 8 Bohr, and the f increase is always accompanied by a swelling of the delocalization tails. The maximum f values are obtained for switching distances between 5 and 6 Bohr, that is, comparable with d_{RB-RB}, and in these cases the swelling is so strong that the reference state can become a fully DE state.

Moreover, the modification of the ES manifold (Figure S8, Panel C) clearly indicates that the dealing parameter in determining the ES relative energy ordering is γ, being the 100% LR HF eX not sufficient for keeping the CT states above the DE ones. In particular, switching distances higher than d_{RB-RB} stabilize the

CT states moving them below the DE ones, while the opposite trend is observed for switching distances lower than d_{RB-RB}.

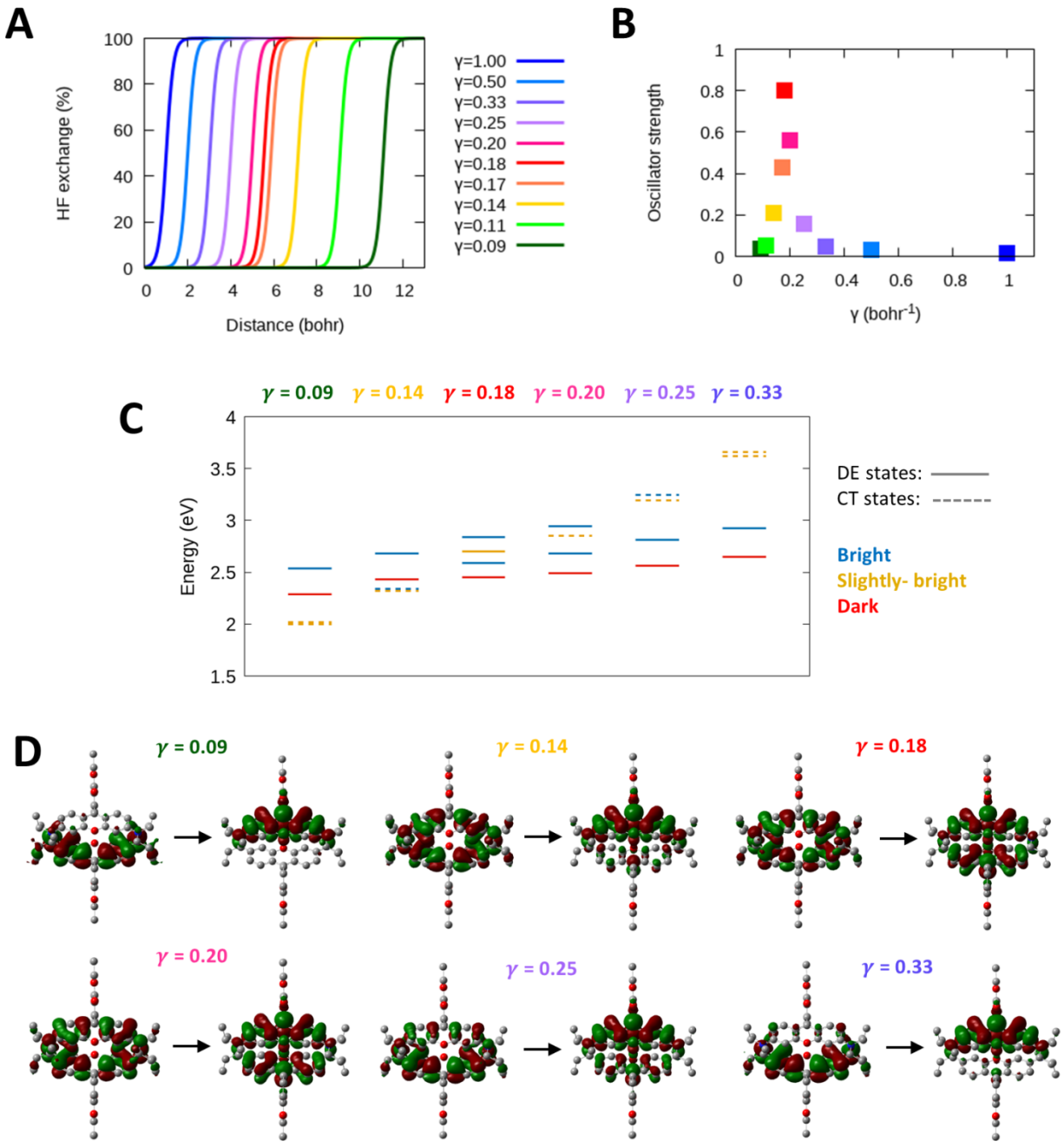

Figure S8. Results of the γ-scan performed within the condition α = 0, β = 1. Panel A: sigmoidal functions qualitatively describing the variation the HF eX as a function of the inter-electronic distance. Panel B: f values obtained for the reference state. Panel C: energy diagrams related to some selected γ values. Panel D: NTOs corresponding to the reference states obtained for the selected γ values.

In what follows, we will analyze the combined effect of SR and LR HF eX by considering the γ values 0.50, 0.20 and 0.11, which corresponds to switching distances that are, respectively, smaller, comparable, and

higher than d_{RB-RB}. We limited the SR HF eX variations from 0% to 40%, because this is the range of values that can be considered physically meaningful within the RS concept.

First, we focus on the effect of including some SR HF eX within the the $\alpha + \beta = 1$ condition. Figure S9 reports the f's evolution obtained upon increasing the SR HF eX with the three chosen γ. For the switching distance smaller than d_{RB-RB} (γ = 0.5) a low f is always obtained independently from the SR HF eX amount. For the switching distance comparable to d_{RB-RB} (γ = 0.18), instead, the increasing of the SR HF eX reduces f. Finally, for the switching distance higher than d_{RB-RB} (γ = 0.11) we found that, upon increasing the SR HF eX, f increases until it reaches a strong maximum at SR HF eX = 30% and then decreases.

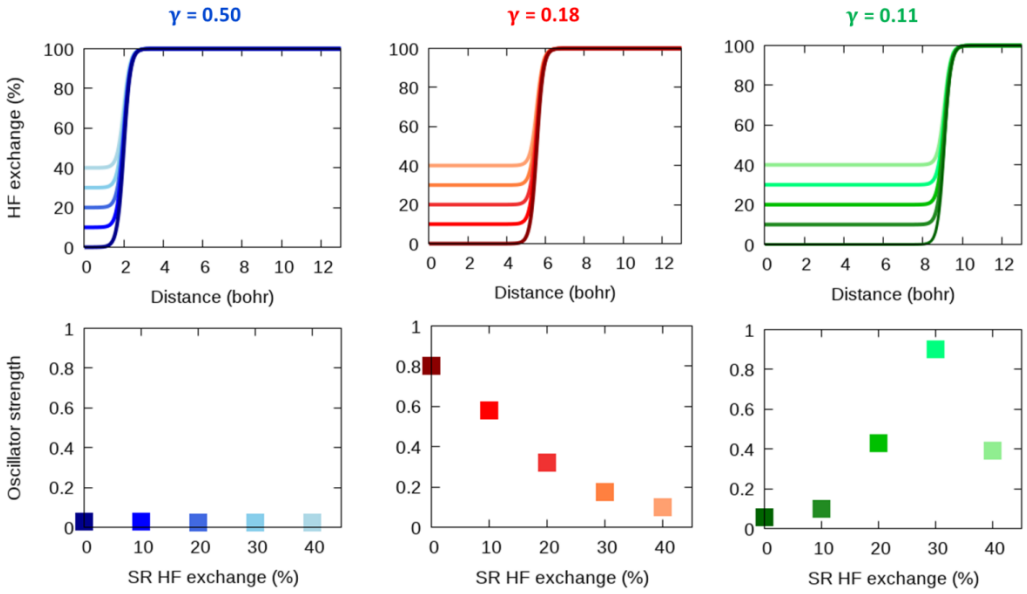

Figure S9. Results of the SR HF eX scan performed within the condition LR HF eX = 100%.

The results obtained so far allow for a straightforward identification of the conditions that trigger the CT delocalization. The most crucial parameter turns out to be γ, because the associated switching distance can lead to very different results depending on whether it is comparable with d_{RB-RB} or not. In particular, three different limiting cases can be identified for the description of the CT states.

The first limiting case leads to a well-defined CT state with low brightness and corresponds to the introduction of a 100% HF eX at d_{RB-RB}, therefore, it will be referred to as the "HF limit". This limit can be reached within the $\alpha + \beta = 1$ condition by fixing a switching distance lower than d_{RB-RB}, which ensures the eX interaction between electrons separated by d_{RB-RB} to be mainly of the HF type independently of the SR HF eX amount (see Figure S9, panel A).

Also, the second limiting case leads to a well-defined CT state with low brightness, but this time the functional feature responsible for such a description is completely different: indeed, this limiting case corresponds to the introduction of a 0% HF eX at d_{RB-RB}, and will be therefore referred to as the "local limit". This limit can be reached within the $\alpha + \beta = 1$ condition by fixing a switching distance higher than d_{RB-RB} (but still lower than the size of the system) along with a very small SR HF eX, which ensures the eX interaction between electrons separated by d_{RB-RB} to be mainly of the DFT type independently of the LR HF eX amount (see the case with SR HF eX = 0-10% in Figure S9, panel C).

The third case, instead, leads to the complete turning of the CT state into a strongly bright DE state and corresponds to the introduction of a very equilibrated mixture of HF and DFT eX at d_{RB-RB}, and will be therefore referred to as the "intermediate HF-DFT limit". This limit can be reached within the $\alpha + \beta = 1$ condition by fixing a switching distance comparable to d_{RB-RB} along with SR FH eX = 0% or by introducing a higher switching distance but with a sensible amount of SR HF eX (see the case with SR HF eX = 30% in Figure S9, panel C).

Having recognized such limits, it is now evident that Figure S8 straightforwardly represents the switching from the HF to the intermediate HF-DFT and then to the local limits, while the panel C of Figure S9 represents the inverse path.

We conclude our analysis of the interplay between the RS parameters by considering also the $\alpha + \beta < 1$ condition.

Figure S10 reports the SR HF eX scan performed at different LR HF eX amounts (that is, 100%, 60%, 40% and 20%) with γ = 0.50. The main outcome is that when the switching distance is lower than d_{RB-RB}, the leading parameter is always the LR HF eX, while the SR eX plays only a secondary role because its effect is strongly limited by the very low switching distance. The reducing of LR HF eX from 100% to 40% produces an increase of f that represents the moving from the HF to the intermediate HF-DFT limit, while the further reducing to 20% inverts the trend indicating the approaching of the local limit.

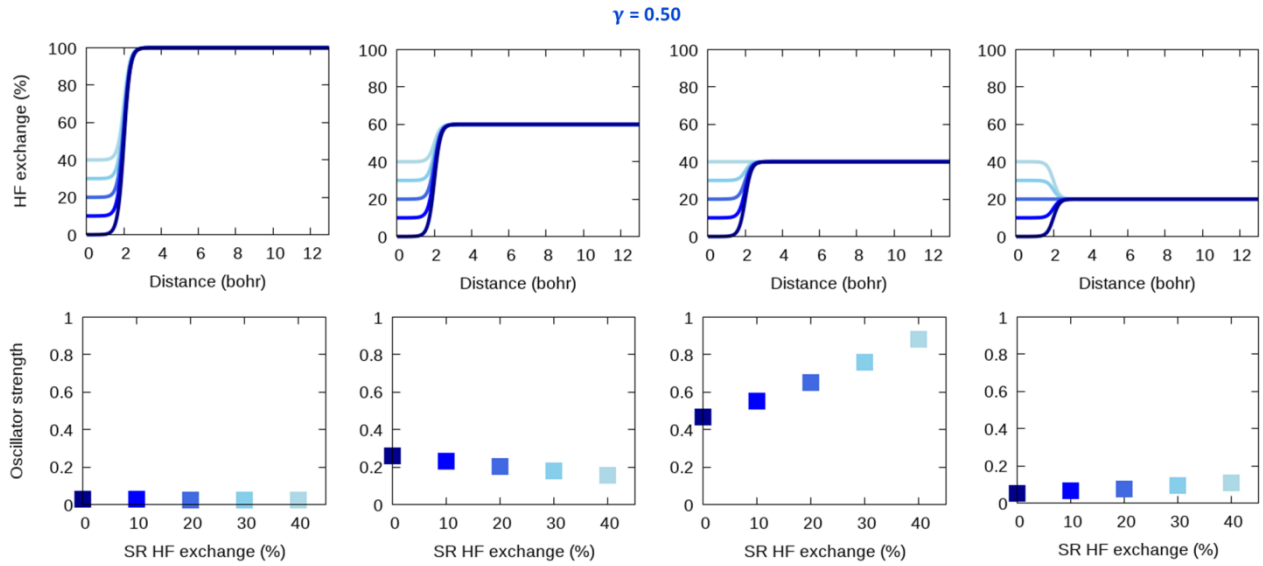

Figure S10. Results of the SR HF eX scans performed for γ = 0.50 within the conditions LR HF eX = 100%, 60%, 40% and 20% (from left to right).

Figure S11 reports the same scan but performed with γ = 0.18. In this case, the main outcome is that when the switching distance is comparable to d_{RB-RB}, there can be a strong competition between effects of the SR and LR HF eX amounts, in particular when the latter takes intermediate values. The detailed commenting of this figure would not add anything new with respect to what observed so far; we limit ourselves to observe that, in all cases, the f modifications can be easily traced back to the switching between the three limiting cases above mentioned.

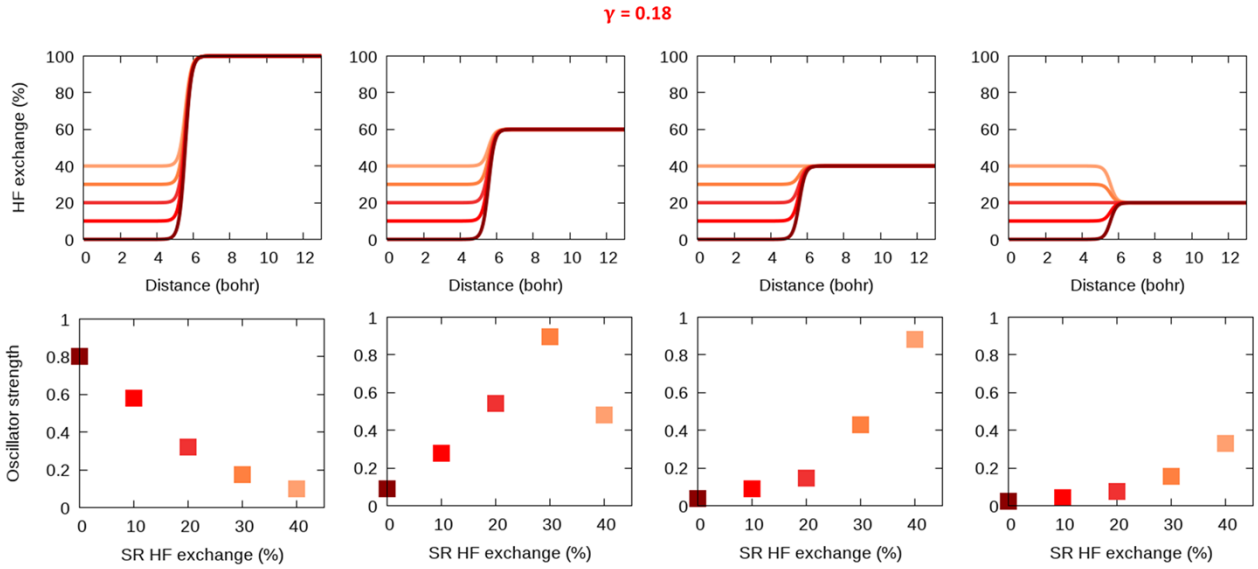

Figure S11. Results of the SR HF eX scans performed for γ = 0.18 within the conditions LR HF eX = 100%, 60%, 40% and 20% (from left to right).

Finally, Figure S12 reports scan performed with γ = 0.11. This time, the main outcome is exactly the opposite with respect to the scan performed with γ = 0.50: when the switching distance is higher than d_{RB-RB}, the effect of the SR HF eX dominates that of the LR HF eX. In particular, the SR HF eX increase from 0% to 40% can move the system from the local to the intermediate HF-DFT limit independently from the fact that the LR HF eX is 20% or 60%.

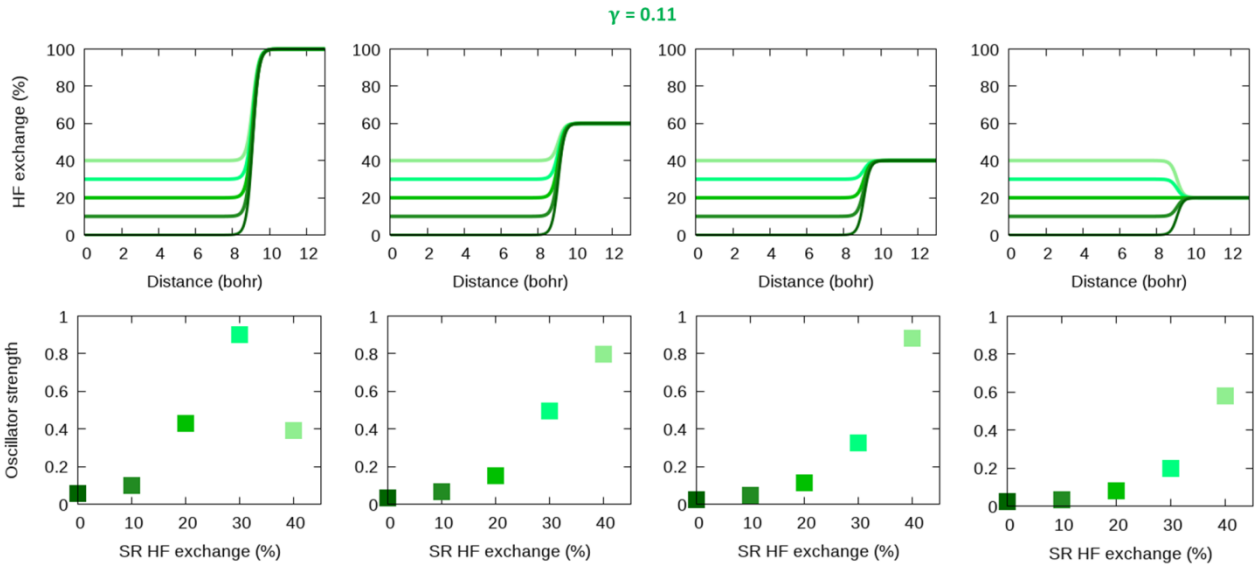

Figure S12. Results of the SR HF eX scans performed for γ = 0.11 within the conditions LR HF eX = 100%, 60%, 40% and 20% (from left to right).

The scans discussed above clearly indicate that the intermediate HF-DFT limit can be generally reached also by simply introducing a proper amount of constant HF eX (hybrid functional parametrization). Figure S13 reports a full-range HF eX scan; the CT state becomes clearly bright when introducing 30-50% of HF eX, with

the maximum f value corresponding to 40%. This result confirms that the reaching of the intermediate HF-DFT limit does not require any specific RS parametrization, being dictated exclusively by the amount of HF eX introduced at distances comparable to d_{RB-RB}, which can be introduced also at the hybrid parametrization level.

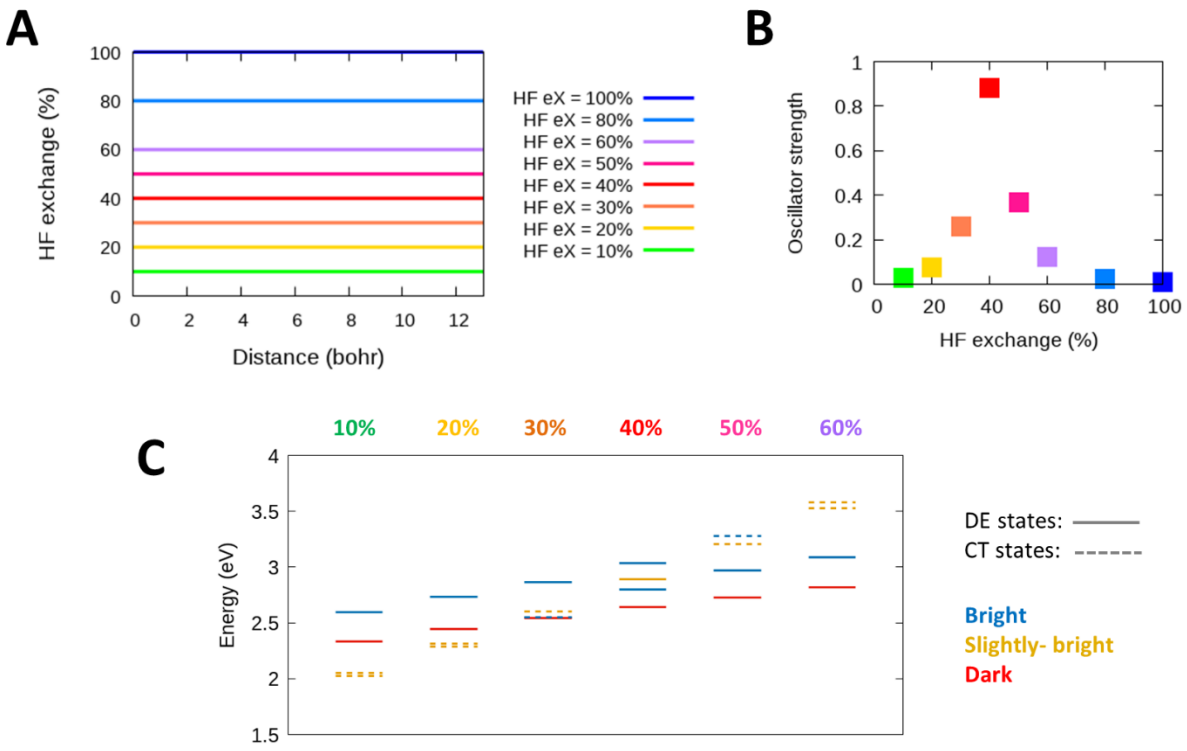

Figure S13. Results of the full-range HF eX scan. Panel A: full-range HF eX as a function of the inter-electronic distance. Panel B: f values obtained for the reference state. Panel C: energy diagrams related to some selected HF eX amounts.